

Stress relaxation of a patterned microstructure on a diaphragm

D.W. Zheng^{a)}

Department of Materials Science and Engineering, University of California at Los Angeles, Los Angeles, California 90095-1595

X.H. Wang and K. Shyu

Manifold Engineering, City of Industry, California 91748

C. Chen

Department of Materials Science and Engineering, University of California at Los Angeles, Los Angeles, California 90095-1595

C-T. Chang

Manifold Engineering, City of Industry, California 91748

K.N. Tu

Department of Materials Science and Engineering, University of California at Los Angeles, Los Angeles, California 90095-1595

A.K. Mal

Department of Mechanical and Aerospace Engineering, University of California at Los Angeles, Los Angeles, California 90095-1595

Y.F. Guo

Advanced Interconnect and System Laboratory (AISL), Semiconductor Product Sector (SPS), Motorola Corp., Tempe, Arizona 85204

(Received 16 December 2001; accepted 25 April 2002)

Stress relaxation of a patterned thin film on diaphragms of different material and thickness was investigated through experimental study and numerical simulation. The diaphragm deflections, caused by relaxation of the residual stress in a patterned thin film residing on top, were measured using a Twyman–Green laser interferometer. The first diaphragm used was a $\text{Si}_3\text{N}_4(\text{top})/\text{SiO}_2/\text{Si}$ composite diaphragm and the second a 0.5- μm -thick Si_3N_4 membrane. Custom-written simulation software, which uses a novel numerical algorithm named Nonlinear Sequential Analysis (N-LISA), was utilized to calculate the stress distribution in the patterned thin film and the diaphragm substrate. Agreement between the model and the experimental results was satisfactory. Simulation of the system balance between a tensile-stressed circular Ti film and a stress-free Si substrate of different thickness clearly shows a transition in the substrate behavior from a pure plate to a pure membrane. Interestingly, the deflection of the Si substrate caused by the residual stress in the Ti film reaches its maximum at a certain substrate thickness where plate and membrane characteristics coexist. This study addresses some basic mechanics issues involved in modern devices dealing with thin diaphragms.

I. INTRODUCTION

Stress relaxation of a patterned thin film on a substrate is a fundamental solid mechanics problem, which finds many important applications in modern microelectronics. Although the interaction of a stressed thin film with a thick substrate is well understood, the interaction of a patterned and stressed thin film with a thin substrate has not been carefully investigated. Currently, there is an

urgent need to thoroughly understand such a system to facilitate the research and development of many critical technologies.

One important application lies in the image placement of an x-ray mask used for deep-sub-micron lithography. Here the system typically consists of a thin Si diaphragm (e.g., 2 μm thick) or silicon nitride film, which supports a layer of patterned high-Z absorber material. As the supporting substrate thins down to a membrane, both the bending and in-plane elongation of the substrate need to be considered and the stresses in the system become much more complicated. As pointed out by the review

^{a)}Present address: Lightcross, Inc., 2630 Corporate Place, Monterey Park, CA 91754.
e-mail: dzheng@lightcross.com

articles,^{1,2} the x-ray mask itself is the most critical and difficult system element of x-ray lithography. The diaphragm as well as the absorber materials has residual stresses. The in-plane distortion of the diaphragm caused by stress relaxation of the absorber material has to be corrected to improve the overall accuracy to meet the stringent total error tolerance of 45 nm for 0.13 μm complementary metal-oxide semiconductor (CMOS) devices.³ One practice utilized by researchers is to fabricate an exploratory mask, measure the movement of fiducials distributed on the mask, and record the error.^{4–7} This information is then fed back to the original mask design to reflect the mask pattern shift due to stress. Significant improvement has been achieved through this approach. Nevertheless, it is obviously more economical to use simulations to predict these numbers, and several efforts are underway for the development of such a software.^{8–10}

Interaction of a prestressed and patterned thin film with a thin substrate is also quite typical in the field of micro-electro-mechanical-system (MEMS) devices.^{11–14} A patterned film residing on top of a diaphragm or beam supported either at four edges or one side is quite typical in various MEMS devices. Knowledge of the stress in various films, and the deflection of the supporting diaphragm or beam caused by this residual stress, is important for initial device design and long-term reliability. As an example, Fig. 1(a) displays a schematic diagram showing the cross-sectional view of a CO chemical sensor. A top view optical image of the sensor is presented as Fig. 1(b). The deflection of the supporting Si diaphragm caused by the stress in various metal lines was captured by a Twyman–Green laser interferometer^{15,16} and the fringe images are given in Fig. 1(c).

In summary, from the device process integration point of view, two things are of key concern. One is how much wafer deformation occurs due to the stress in various layers, the other is the possible stress reduction due to membrane response. An example of the latter is the stress in e-beam evaporated nickel (Ni). Typically its thickness on a regular wafer is limited to about 2500 Å. However, if Ni is deposited onto a membrane, a significant stress reduction might occur, resulting in more relaxed process constraints. Stresses in a patterned microstructure could cause local deflection in the wafer but it is typically not an issue to lithography for generic CMOS devices. However, in MEMS devices, stress relaxation in thin diaphragms could cause significant local deformation in the substrate, which could potentially pose an alignment problem.

In this paper, some experimental evidence is presented, from which a few basic concepts to be used in the numerical modeling are extracted. Then the numerical method is applied to a model where a fixed metal pattern is placed on Si diaphragms of different thickness, and which is difficult to fabricate experimentally. Through

this modeling effort, we are able to understand the basic mechanics behind the interaction of a thin patterned film with residual stress and a thin substrate, where this thin substrate can be multilayered and may have intrinsic stresses.

II. EXPERIMENTAL

A. Sample fabrication

For the sake of comparison, a 0.5- μm -thick Ti film was patterned to different sizes and on top of square diaphragms, which had different thickness as well as number of layers of diverse nature. In all cases, the diaphragms were formed before the Ti film was deposited and patterned.

Fabrication of thin diaphragms with controlled thickness was achieved using thin dielectrics as etch masks. The properties of these samples are described briefly in the following subsections.

1. Fabrication of a 22- μm -thick Si diaphragm

A 400- μm -thick *p*-type (100)Si wafer was used as the starting substrate, on top of which an *n*-type epitaxial layer 22 μm in thickness, (100)Si was grown. Low-temperature oxide (LTO) of 0.35 μm and 0.4 μm of plasma-enhanced chemical vapor deposition (PECVD) $\text{Si}_x\text{N}_y\text{H}_z$ were deposited on both sides of the Si wafer as etch masks. The composition and thickness of the $\text{Si}_x\text{N}_y\text{H}_z$ layer was carefully tuned so the overall bending moment exerted onto the Si substrate by the $\text{Si}_x\text{N}_y\text{H}_z$ and LTO layers and its temperature coefficient was minimized. The Si etching was done using 30 wt% KOH solution at 85 °C. This was due to the excellent (100) over (111) plane etch ratio (greater than 400) compared to tetra methyl ammonia hydroxide (TMAH; less than 50) and EDP (about 35).¹⁷ A constant voltage source reverse-biased the *p-n* junction formed by the *n*-type epi Si and the *p*-type substrate. The etch-end-point was detected when all *p*-type Si was removed as indicated by an abrupt increase in the current. The uniformity of etching was about 0.3 μm across 2750 \times 2750 μm area.¹⁸

2. Fabrication of a 4.6- μm -thick composite Si diaphragm

A 300- μm -thick, (100)Si wafer with 3- μm heavily-boron-diffusion-doped ($5 \times 10^{19}/\text{cm}^3$) top layer (purchased from North Carolina Microelectronics Center, NC) was used as the starting substrate. Wet oxide 0.5 μm in thickness was grown onto the wafer at 1050 °C, followed by a deposition of 0.15- μm LPCVD stoichiometric Si_3N_4 . The residual stress due to the wet oxide and LPCVD nitride blanket film was measured to be –300 MPa compressive and 1 GPa tensile, respectively, using Flexus machine (KLA Tencor Corp, San Jose, CA). The back opening was patterned by first etching the nitride away using $\text{CF}_4:\text{O}_2 = 125:25$ mTorr gas

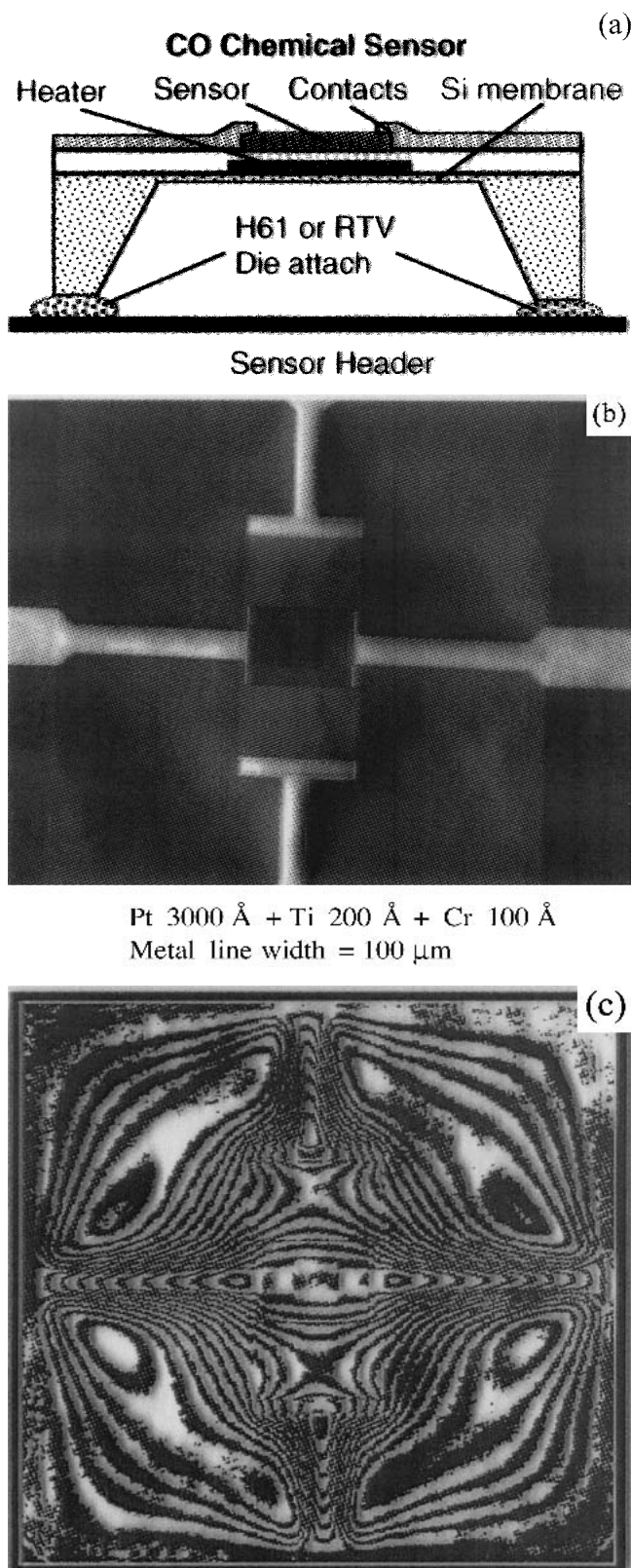


FIG. 1. (a) Schematic view of the cross-section of a CO sensor. (b) Optical microscope image of the top view of the sensor showing the metal layers. (c) Interferometric images showing the deflection of the sensor diaphragm caused by the residual stress in various thin film layers.

chemistry at 200 W for 2.5 min, followed by a wet etch in buffered oxide etchant (BOE) to remove the oxide. This induced an over-etching of nitride and an etching into the oxide layer underneath of only about 1–2 kÅ. The use of BOE wet etchant instead of dry etchant to remove the oxide helped to minimize possible lateral etching during Si wet etch at a later stage. Si was etched first using 30 wt% KOH at 75 °C to a thickness of about 100 μm, and then switched into ethylene diamine pyrocatechol (EDP) solution (purchased from Transene Electronics, Inc., Danvers, MA) at 90 °C with condensation setup. Due to the significant etch rate reduction of EDP when the doping level in Si was degenerated¹⁷ (reduction of about 50 times, when the doping level is higher than $5 \times 10^{19} \text{ cm}^{-3}$), a timed etch was performed to reduce Si thickness to 4.6 μm. The uniformity of the back surface was better than 0.18 μm across a $1600 \times 1600 \mu\text{m}$ area. It was found that if the Si thickness were reduced to about 2.8 μm, then the composite diaphragm $\text{Si}_3\text{N}_4/\text{SiO}_2/\text{Si}$ would start to buckle. Even after the removal of the $\text{Si}_3\text{N}_4/\text{SiO}_2$ bilayer dielectrics, the diaphragm remained buckled, which suggested that some plastic deformation had occurred in the Si diaphragm.¹⁹

3. Fabrication of a 0.5-μm-thick low-stress Si_3N_4 diaphragm

The low-stress nitride diaphragm was among the easiest to fabricate because of the excellent resistance of nitride to KOH, TMAH, and EDP etchants. In this process, a layer of low-stress nitride was deposited onto both sides of the (100)Si wafer, and the backside layer was patterned using the CF_4/O_2 plasma mentioned previously. KOH was picked to etch Si because it has an excellent (100) over (111) plane etch ratio and is less expensive.

B. Analysis of diaphragm deformation

1. Contribution from thin dielectrics

To evaluate the effect from the thin dielectrics, two groups of samples were fabricated for comparison. A half-micron-thick Ti film was patterned into dot (circular) shapes with different diameters on top of the 22-μm composite Si diaphragms, as described in Sec. II. A. 1 (fabrication of a 22-μm-thick Si diaphragm). This makes up Group A. The comparison Group B consisted of pure 22-μm-thick Si diaphragm with dots of patterned Ti residing on top, identical to Group A. Group B samples were simply made by removing the dielectric layers from the Group A sample; the cross-sectional schematics are shown in Figs. 2(a) and 2(b). After image processing, the diaphragm deflection along a half meridian, caused by the residual stress in the Ti film, is plotted as Fig. 2(c). The diaphragm deflections with and without the dielectrics can be seen to be significantly different.

One distinction between Group A and Group B samples is that the 22- μm -thick Si diaphragm behaves like a plate, while the composite sample behaves like a plate bonded to a membrane (dielectrics) with residual stress. If we recall the difference between a plate and a membrane,¹⁹ vertical loads in a plate are balanced by bending and shear stresses, while in a membrane, they are balanced by the vertical components of the tensile “membrane stresses” caused by the membrane’s local curvature. In general, when the substrate is relatively thick, e.g., 200 μm or thicker for a 4-in. wafer, the effect from the thin dielectric is negligible. For example, suppose we use a Flexus machine to measure the stresses in multi-layered thin films on a thick wafer. When the stress in the 2nd deposited layer is calculated, the wafer curvature effect from the 2nd layer is typically considered as linearly additive. The bending stiffness of the substrate dominates over the residual stress in the 1st layer. However, in the present case, when the substrate is thinned down to 20 μm , both the bending stiffness of the

substrate and the residual stress of the dielectric coatings have to be considered. On the other hand, there is obviously an increase in the overall bending stiffness due to the presence of the thin dielectrics. However, considering that (i) the Young’s moduli of the 3 materials are in a decreasing sequence of nitride (270 Gpa), Si (169 Gpa), SiO_2 (72.9 Gpa); (ii) the thickness of Si is much larger than the other 2 dielectrics Si (22 μm), SiO_2 (0.4 μm), Si_3N_4 (0.35 μm), and (iii) the bending stiffness is inversely proportional to the flexural rigidity EI where E and I are the Young’s modulus and area moment of inertia of the cross section respectively, this effect is probably not adequate to explain the change of diaphragm deflection alone.

2. Effect of the overall bending moment

For comparison purposes, two additional groups of samples were fabricated and named Groups C and D. Group C consists of samples based on the description of Sec. II. A. 2. A schematic diagram of the cross-section of this group is plotted in Fig. 3(a). Group D is different in the sense that the pad oxide used was reduced from 0.5 to 0.1 μm ; the schematic diagram of the cross section of this group is shown in Fig. 4(a). Identical Ti dots were patterned on top of these diaphragms, whose deflection caused by the residual stress in the Ti pattern are displayed in Figs. 3(b) and 4(b), respectively.

As previously discussed, considering the residual stress level in LPCVD Si_3N_4 and wet thermal oxide, it appears that the bending moment exerted onto the thin Si

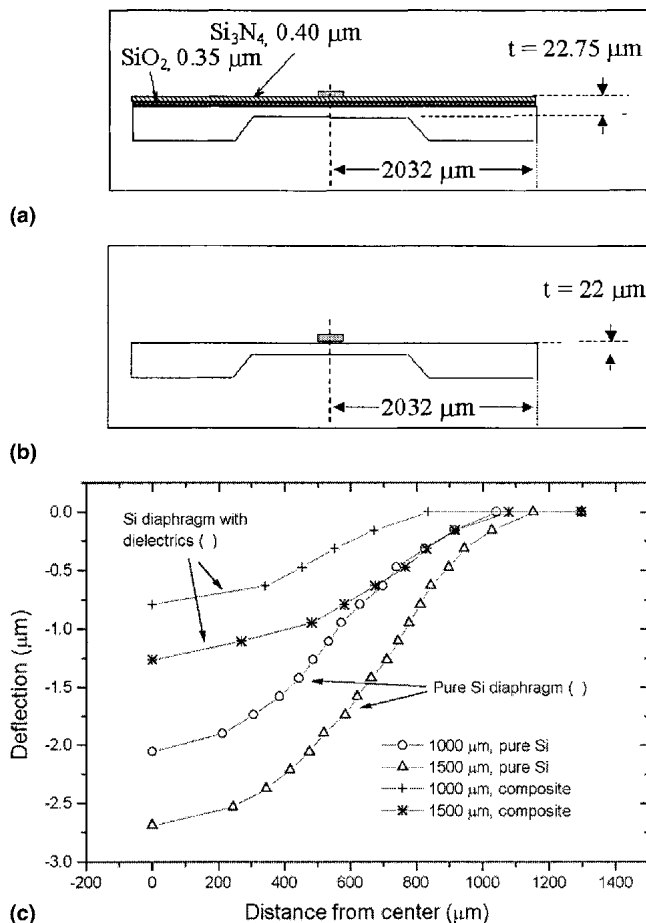


FIG. 2. Schematic diagram of the cross-section of (a) a composite Si_3N_4 (0.16 μm) SiO_2 (0.5 μm)/Si (22 μm) Si diaphragm, and (b) a 22- μm Si diaphragm. (c) Comparison of total diaphragm deflection caused by the residual stress in the Ti dot pattern residing on top: (Group A) pure Si diaphragm, (Group B) Si diaphragm with dielectric capping layer.

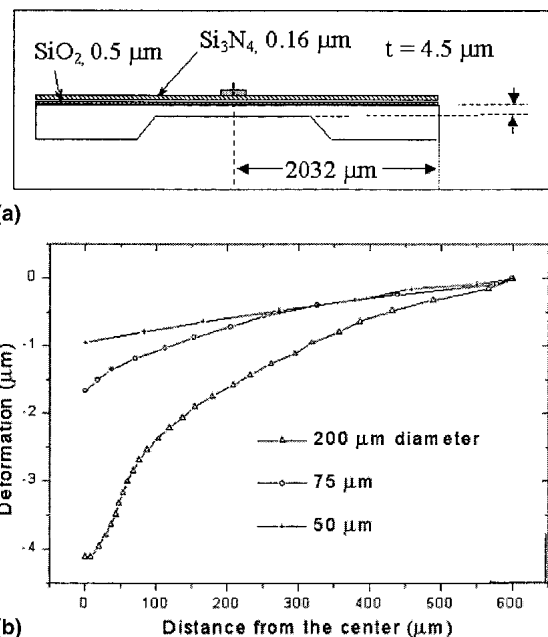


FIG. 3. (a) Schematic diagram of the cross-section of a composite Si_3N_4 (0.16 μm)/ SiO_2 (0.5 μm)/Si diaphragm. (b) Deflection curve of the diaphragm caused by the residual stress in the Ti dot pattern residing on top.

substrate is balanced better in the case of Group C sample. In contrast, Group D has unbalanced bending moment from the tensile stress in the Si_3N_4 . We believe this is the main reason why the substrate bending is much smaller for the latter case, because more is needed to rotate the unbalanced in-plane tensile stress. On the other hand, as in the previous case (Sec. II. B. 2), there is a difference in the overall bending stiffness due to the Si_3N_4 layer. The contribution from the stresses in the dielectric layer needs further investigation.

3. Stress relaxation on a pure membrane

Similar to the previous case, a Ti blanket film was e-beam evaporated onto a 0.5- μm -thick LPCVD Si_3N_4 diaphragm described in Sec. II. A. 3 and patterned to dots 1000, 100, and 50 μm in diameter. A schematic cross-sectional view of the sample is provided as Fig. 5(a), and the deflection of the supporting diaphragm is displayed in Fig. 5(b).

Comparing the deflection profile of the thin Si_3N_4 diaphragm with what was observed in the former cases, the diaphragm has no deflection immediately below the Ti pattern and far from the Ti pattern; only the area of the diaphragm immediately below the edge of the Ti pattern has a drastic change in shape. Recalling that in a membrane, external vertical loads are balanced by rotation of the in-plane stress, this thin nitride diaphragm behaves primarily like a pure membrane. The membrane does not bend outside the Ti pattern area, because its

bending stiffness is negligible. It has a very steep slope around the Ti pattern edge due to the residual stress in the Ti pattern, and the bending stiffness of the membrane does play a role in this very local area.

III. ANALYSIS OF THE THIN DIAPHRAGM DEFLECTION

It is well known that as the thickness of the substrate decreases, the behavior of the substrate changes from a plate effect dominated behavior to a membrane effect dominated behavior. Based on the observations in Sec. II, for a relatively thick Si substrate, the residual stress in a pattern residing on top would bend it to the shape of a relatively low-order polynomial. On the other hand, for an ultrathin nitride membrane, the deformation of the substrate occurs only in a localized area immediately below the edge of the pattern. Particularly for the latter case, modeling efforts would be very helpful in understanding the mechanics of the deformation in that localized area, since very steep rotation of the membrane could result in very high stresses. It is apparent that for certain substrate thicknesses both the plate effect (substrate bending stiffness) and the membrane effect (rotation of the residual stress in a membrane to balance external force) can play a role. The mathematical formulation of the associated nonlinear boundary value problem is well known²¹ and will not be repeated. In the present problem, where the maximum vertical deflection is much smaller than the radial dimensions of the plate, the formation leads to the well known von Kármán

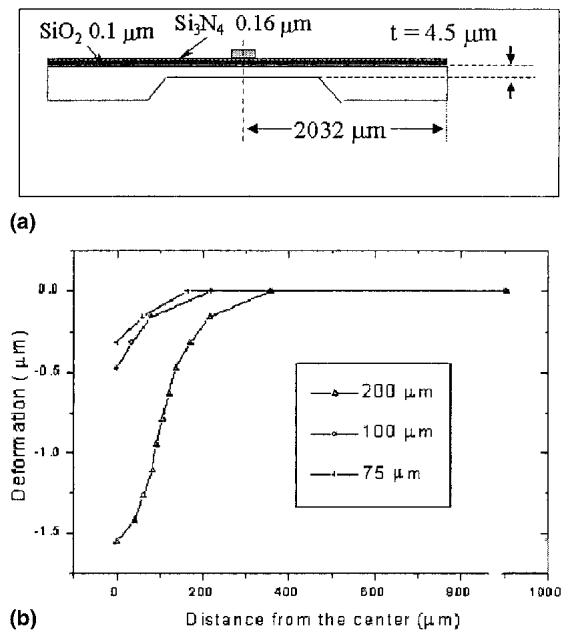


FIG. 4. (a) Schematic diagram of the cross-section of a composite Si_3N_4 (0.16 μm)/ SiO_2 (0.1 μm)/Si diaphragm. (b) Deflection curve of the diaphragm caused by the residual stress on the Ti dot pattern residing on top.

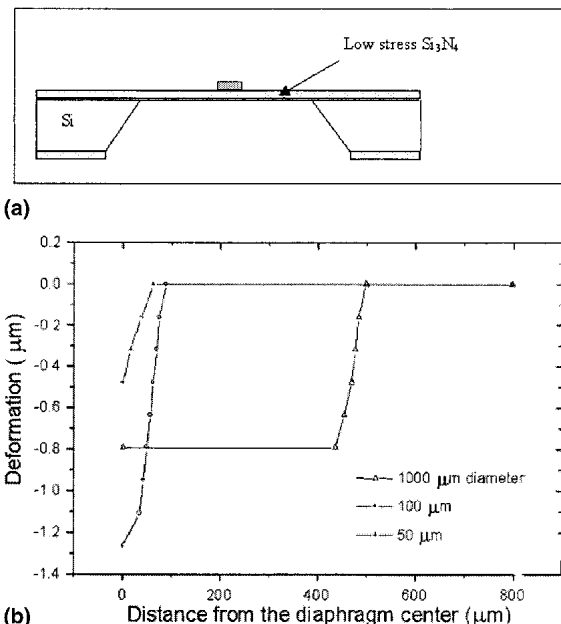


FIG. 5. (a) Schematic diagram of the cross-section of a low-stress Si_3N_4 (0.5 μm) diaphragm. (b) Deflection curve of the diaphragm caused by the residual stress in the Ti dot pattern residing on top.

equations²¹ with fixed conditions at the diaphragm boundary. Since the equations are highly complex and nonlinear, they need to be solved numerically.

An algorithm named Nonlinear Sequential Analysis (N-LISA) has been recently developed to solve the von Kármán equations based on the modified steepest descent method and the initial stress method.^{22,23} The two methods form the basic framework of N-LISA; however, a few additional features have been introduced in the approach utilized in this paper. The domain discretization procedure and the formation of the basic algebraic equations in N-LISA follow that of the finite element method (FEM). For nonlinear deformation of a thick diaphragm, which includes the in-plane membrane stresses as well as the bending stresses of the plate, there are usually many stationary points in the solution space of the algebraic equations depending on the specific problem. Thus the trial solution can easily converge to stationary points other than the real solution during iteration cycles. To avoid this, the following steps were taken.

First of all, the residual stress in the thin film pattern was divided into many portions, which were unevenly partitioned. At the beginning, a very small portion was applied and the corresponding solution was calculated, and this was called one sequence. Then the residual stress value was added and obtained the solution; this was repeated until the deformation corresponding to the real residual stress in the pattern was reached. The reason for this is that the capability of the diaphragm to resist the external load is quite sensitive to the shape of the diaphragm, especially for the high residual stress system. We have observed that during the numerical experiment, too fast of a loading at the beginning leads the iteration solution to converge to a deformation shape, which has many local ripples. On the other hand, within one sequence, the convergence of the problem with a differential loading on top of the deformation shape from the previous sequence step was good. The details of the numerical simulation will be published elsewhere.

To gain some physical insights into our problem, a virtual case was simulated. A circular, 0.5- μm -thick, 100- μm -diameter Ti disc was patterned on top of a circular Si diaphragm with a radius of 1380 μm . Such a geometry would allow an axisymmetric model to be utilized. The boundary was assumed to be fixed, and an in-plane normal initial stress of 337 MPa was assigned to the Ti disc, which corresponded to the real value measured from e-beam deposited samples. The Si diaphragm was assumed to be stress-free; the other material properties used in the model are listed in Table I. The problem is clearly axisymmetric. The thickness of the Si diaphragm was allowed to vary, and the calculated deflections of the Si diaphragm are plotted in Figs. 6(a) and 6(b). Since the Si diaphragms used in this simulation do not have residual stress, the diaphragm transition from a

pure plate to a pure membrane effect could be identified clearly. In Fig. 6(a), as the Si diaphragm thickness decreases from 10 to 3 μm , its deflection increases, as can be expected. However, as the Si diaphragm thickness decreases further, the maximum diaphragm deflection starts to decrease, as can be seen in Fig. 6(b).

At a thickness of 0.5 μm , the Si diaphragm deforms locally, and the effect from a prestressed pattern sitting on top only propagates roughly within a distance of $2R$, where R ($= 100 \mu\text{m}$) is the radius of the Ti pattern. This

TABLE I. Summarization of the material mechanical properties used in the simulation.

Material	Young's modulus (GPa)	Poisson's ratio	Residual stress (MPa)
Ti	110	0.31	337
Si ₃ N ₄ (stoichiometric)	270	0.27	1000
SiO ₂	72.9	0.17	-300
Si	169	0.28	0
Si ₃ N ₄ (low stress)	270	0.27	28.54

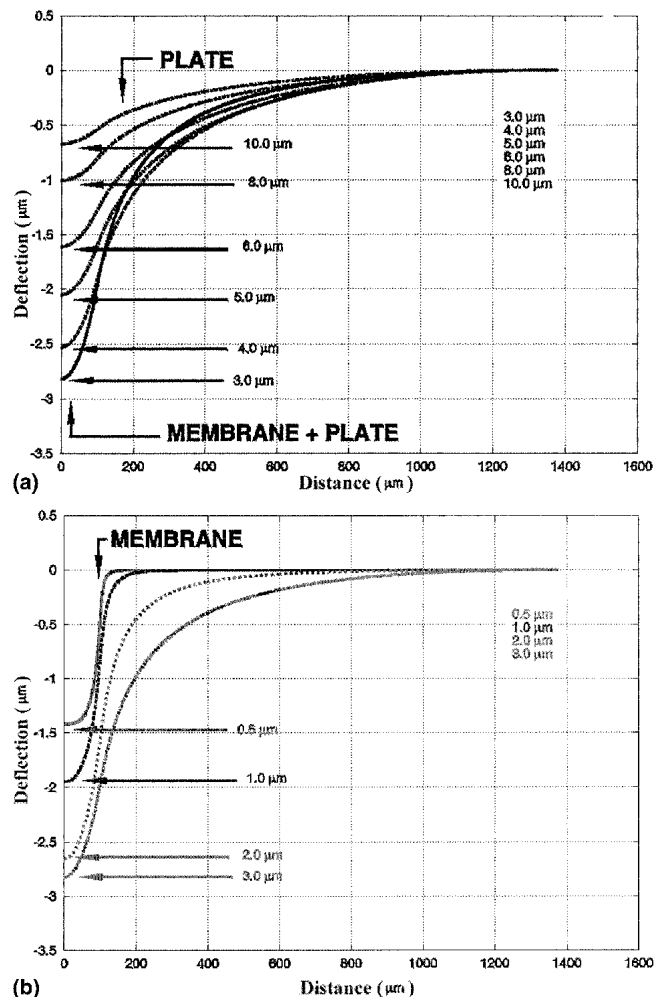


FIG. 6. The Si diaphragm deflection caused by a 100- μm -diameter pad residing on top. (a) Si diaphragm thickness ranges from 10 to 3.0 μm . (b) Si diaphragm thickness ranges from 3 to 0.5 μm .

curve is labeled “MEMBRANE” in the plot. If we look at the diaphragm deflection profile for the case of the Si thickness of $3.0\ \mu\text{m}$, it is a combination of the “PLATE” and “MEMBRANE” type of deformation curve, and is therefore a combined “MEMBRANE + PLATE” case, as marked in the figure. It is interesting to note that in this transition region, the Si diaphragm’s total deflection reaches its maximum. If we plot the total deflection of the Si diaphragm versus its thickness, we obtain the open dots shown in Fig. 7. To see the effect of the residual stress, we fixed all other conditions except the Si diaphragm’s residual stress, which was arbitrarily assigned

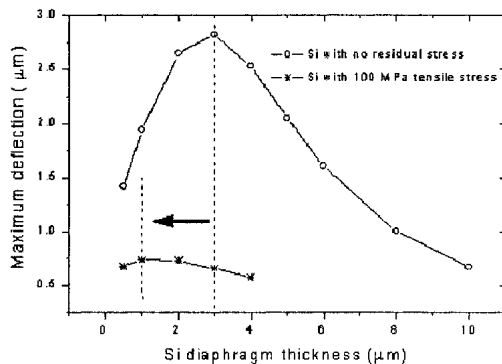


FIG. 7. The maximum of Si diaphragm deflection, caused by the stress relaxation of a pre-stressed Ti pattern residing on top, versus the diaphragm thickness.

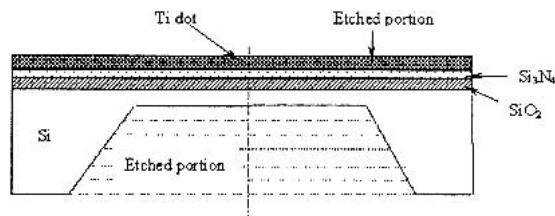


FIG. 8. The schematic cross-sectional view of a test sample, which consists of a Ti pattern residing on $\text{Si}_3\text{N}_4/\text{SiO}_2/\text{Si}$ composite diaphragm.

as 100 MPa (tensile). Again the total deflection of the Si diaphragm is plotted against its thickness, which is shown by the stars in Fig. 7. It is very clear that the presence of a tensile residual stress will decrease the total diaphragm deflection, and it also shifts the diaphragm thickness corresponding to the maximum deflection to a smaller value.

Now it is time to look into the real and more difficult cases mentioned in Sec. II. The $200\text{-}\mu\text{m}$ -diameter Ti pattern of Sec. II. A. 2 is selected for study. The simulation procedure is as follows. Since we could not stimulate the deposition of a blanket film on a diaphragm, we assume that the film was deposited on a bulk substrate and then the Si was etched from the bottom to form a diaphragm. An initial stress was assigned to the oxide to achieve a compressive stress value of 300 MPa after stress relaxation on a bulk Si substrate, which was $525\ \mu\text{m}$ thick. This procedure was repeated for nitride and Ti film to obtain their corresponding residual stress in accordance with the Flexus-machine-measured values. Then the Si, as outlined by the dashed lines in Fig. 8, is removed layer-by-layer using the numerical etching algorithm.^{19,24} Similar work was done to the Ti film, which was partially etched eventually. At this stage, the composite diaphragm deflection could be calculated and converted to equivalent interferometric fringes assuming that the diaphragm center is the brightest spot. Since only an axisymmetric model was available, the calculated fringes were bounded within a circle. A comparison between the experimental and numerical fringe images for this case is presented in Fig. 9. The results obtained are qualitatively similar. Therefore, it seems that our simulation approach is reasonable.

The thin low-stress nitride diaphragm described in Sec. II. A 3 is another interesting case for modeling. The nitride diaphragm is a half-micron thick, so a laser light can penetrate through it and reflect off the Ti/nitride interface. A very thin coating of e-beam Al of about

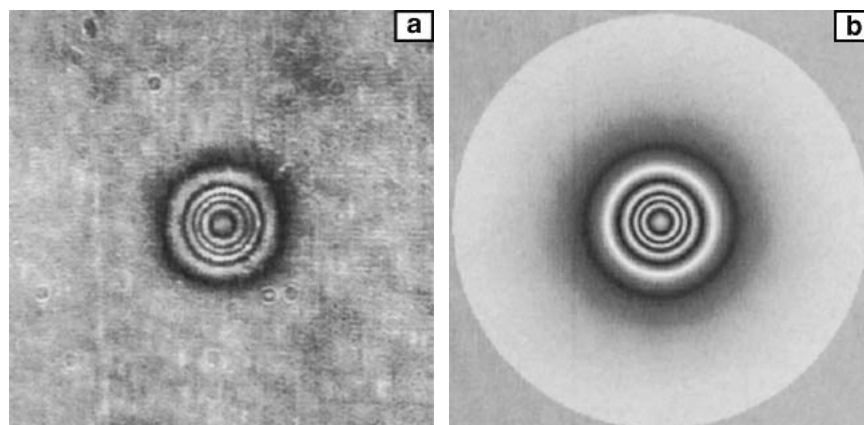


FIG. 9. A comparison between the calculated and the experimental fringe pattern for a $200\text{-}\mu\text{m}$ -diameter Ti dot on a $4.5\text{-}\mu\text{m}$ -thick composite Si diaphragm: (a) experimental, (b) simulated.

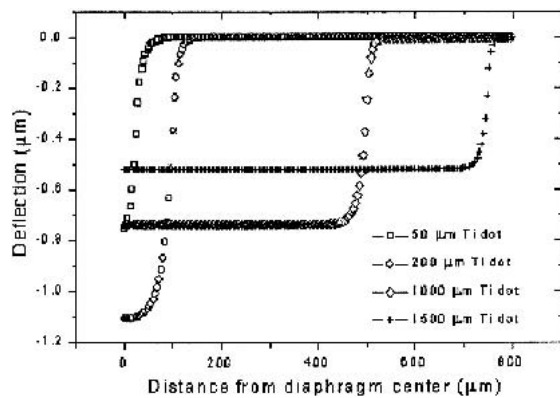


FIG. 10. Calculated low-stress nitride deflection caused by a stressed Ti pattern residing on top.

200 Å does not improve this situation. Therefore, while the overall deformation of the nitride diaphragm could be identified unambiguously, the situation around the Ti bump edge is not clear. This is a situation in which this simulation could help in gaining some insight. The residual stress of the nitride film was measured using the bulge-testing method.^{19,20} The mechanical properties used for low-stress nitride and Ti are given in Table I. The simulation result is displayed as Fig. 10. It is obvious that the general shape of the calculated and measured deflection curves match very well. Since the interferometric image does not have sufficient resolution to distinguish between the calculated curve of Fig. 10 and the measured curve of Fig. 5, and since our model is axisymmetric while the real diaphragm is a square, a direct comparison between the two cases was not attempted.

IV. CONCLUSION

The deflection of a diaphragm of different thicknesses caused by the residual stress in a patterned thin film residing on top was studied experimentally and modeled using numerical simulation. The transition of the diaphragm behavior from a pure plate, to plate plus membrane, and then to a pure membrane is clearly shown using numerical simulations. The numerical model was supported by experimental measurements of the out-of-plane deformation of such a diaphragm. We found that at certain diaphragm thickness, the diaphragm's total deflection reaches a maximum with fixed residual stress in the pattern sitting on top. A tensile stress in the diaphragm would shift this peak position and reduce the total deflection.

ACKNOWLEDGMENTS

Manifold Engineering and the University of California at Los Angeles acknowledge the support from the National Science Foundation under Small Business

Initiative Reward (SBIR) Contract No. 9960511. The authors are grateful to Jordan Neysmith and Bernard Hart from ELOtechnologies, Inc., Torrance, CA, for the proofreading of this paper.

REFERENCES

1. R.E. Acosta, "A review of deposition, patterning, and stress of metal films used as absorber in masks for synchrotron X-ray lithography", in *Proceedings of the Second International Symposium on Electrochemical Microfabrication*, edited by M. Datta, K. Sheppard, and J.D. Dukovic (Electrochemical Society, Pennington, NJ, 1995), p. 88.
2. J. Silverman, *J. Vac. Sci. Technol. B* **15**, 2117 (1997).
3. 1997 Semiconductor Industry Association Roadmap, Sematech, Austin, TX.
4. S. Tsuboi, Y. Yamashita, T. Matsuo, T. Ohta, T. Shoki, T. Yoshihara, T. Taguchi, S. Mitsui, S. Noda, K. Suzuki, H. Hoga, Y.I. Yamaguchi, and K. Suzuki, *Jpn. J. Appl. Phys.* **35**, 2845 (1996).
5. A.H. Fisher, M.F. Laudon, R.L. Engelstad, E.G. Lovell, and F. Cerrina, *J. Vac. Sci. Technol. B* **15**, 2249 (1997).
6. W.J. Dauksher, D.J. Resnick, K.D. Cummings, J. Baker, R.B. Gregory, N.D. Theodore, J.A. Chan, W.A. Johnson, C.J. Mogab, M-A. Nicolet, and J.S. Reid, *J. Vac. Sci. Technol. B* **13**, 3103 (1995).
7. S.C. Nash and T.B. Faure, *J. Vac. Sci. Technol. B* **9**, 3324 (1991).
8. M. Oda, S. Uchiyama, and T. Matsuda, *Jpn. J. Appl. Phys.* **35**, part I, 6469 (1996).
9. S. Uchiyama, M. Oda, and T. Matsuda, *J. Vac. Sci. Technol. B* **14**, 4332 (1996).
10. M. Laudon, A. Fisher, R. Engelstad, F. Cerrina, K. Cummings, W. Dauksher, D. Resnick, W. Johnson, and D. Puisto, *Microelectron. Eng.* **35**, 549 (1997).
11. G.F. Cardinale, D.G. Howitt, W.M. Clift, K.F. McCarty, D.L. Medlin, P.B. Mirkarimi, and N.R. Moody, *Thin Solid Films* **287**, 214 (1996).
12. G.F. Cardinale, D.G. Howitt, K.F. McCarty, D.L. Medlin, P.B. Mirkarimi, and N.R. Moody, *Diamond Relat. Mater.* **5**, 1295 (1996).
13. E.H. Yang, S.S. Yang, and S.H. Yoo, *Appl. Phys. Lett.* **67**, 912 (1995).
14. X. Ding, W.H. Ko, and J.M. Mansour, *Sens. Actuators A* **21-23**, 866 (1990).
15. *Handbook on Experimental Mechanics*, edited by Albert S. Kobayashi (Society for Experimental Mechanics, Prentice-Hall, Englewood Cliffs, NJ, 1987).
16. D. Zheng, R.P. Hwang, X.Y. Dou, C.P. Yeh, M. Prakash, K. Boardman, and G. Ridsdale, in *Proceedings of 47th Electronic Components and Technology Conference (IEEE, New York, 1997)*, p. 1176.
17. Marc Madou, *Fundamentals of Microfabrication* (CRC Press, Boca Raton, FL, 1997).
18. D.W. Zheng, Xinhua Wang, K. Shyu, C-T. Chang, Y. Guo, V. Sarihan, W. Wen, and K.N. Tu, *J. Vac. Sci. Technol. B* **17**, 2178 (1999).
19. D.W. Zheng, Ph.D. dissertation, University of California at Los Angeles (1999), p. 37.
20. D.W. Zheng, Y.H. Xu, Y.P. Tsai, K.N. Tu, P. Patterson, B. Zhao, Q-Z. Liu, and M. Brongo, *Appl. Phys. Lett.* **76**, 2000 (2002).
21. S. Timoshenko and S. Woinowsky-Krieger, *Theory of Plates and Shells* (McGraw-Hill, Columbus, OH, 1959).
22. O.C. Zienkiewicz and R.L. Taylor, *The Finite Element Method*, 4th ed. (McGraw-Hill, Columbus, OH, 1991).
23. K. Feng, *Numerical Computation Methods* (Defense Industry Press, Beijing, China, 1978, in Chinese).
24. X.H. Wang, K. Shyu, C-T. Chang, D.W. Zheng, and W. Wen, in *Materials Reliability in Microelectronics IX* (Mater. Res. Soc. Symp. Proc. **563**, Warrendale, PA, 1999), p. 243.